ZURICH, SWITZERLAND
6 - 10 OCTOBER 2025

EUROPEAN GEOTHERMAL CONGRESS 2025

Modelling of high temperature well cements for geothermal well integrity predictions

Hieu-Nguyen Hoang[1], Terence Coudert[1], Gunnar Skulason Kaldal[2], Lilja Tryggvadottir[3], Andri Isak Thorhallsson[3,4]

[1] SINTEF Industry, P.O. Box 4760 Torgarden, NO-7465 Trondheim, Norway

[2] ÍSOR - Iceland GeoSurvey, Urdarhvarfi 8, 203 Kópavogur, Iceland

[3]Reykjavik Energy, Bæjarháls 1, 110 Reykjavík, Iceland

[4] Fac. of Ind. Eng., Mech. Eng. and Computer Science, University of Iceland Hjardarhagi 2-6, 107 Reykjavik, Iceland.

Hieu.nguyen.hoang@sintef.no

Keywords: well cement, foam cement, geothermal, well integrity, modelling

ABSTRACT

This study presents a numerical investigation into the mechanical behavior of foam cements used in geothermal wells, particularly focusing on their performance under high-temperature (HT) conditions. Conventional cementing solutions in geothermal wells, such as Portland-based cement, often struggle with maintaining well integrity due to high thermal stresses and casing expansion during well heating. Foam cement, characterized by its lower Young's modulus, hardening modules, and compaction yield pressure, is proposed as an alternative due to its enhanced flexibility and compressibility. This research develops and implements an advanced well-cement model within the CASINTEG software to simulate the response of foam cement in geothermal wells. The model incorporates key factors such as plasticity, temperature-dependent material properties, and the compaction behavior of the cement under HT conditions. The results indicate that foam cement significantly reduces contact pressure at the casing/cement interface, thereby potentially reducing the risk of casing collapse during thermal cycling. Moreover, foam cement facilitates more homogeneous compaction, enhancing the cement's ability to accommodate radial expansion and contributing to overall well integrity. This study highlights the potential of foam cement to improve the long-term performance and safety of geothermal wells, enabling more efficient energy extraction from super-hot geothermal reservoirs.

1. INTRODUCTION

Geothermal energy, a renewable and sustainable resource, involves extracting heat from the Earth's crust. Conventional geothermal wells typically operate at temperatures between 200 and 300°C. However, as energy demand increases, there is growing interest in super-hot geothermal wells (>350°C), which offer the potential for significantly higher energy yields due to their elevated thermal gradients. Operating in such extreme environments, however, presents several technological challenges, particularly regarding the long-term integrity of well materials. A critical component of the well system is the cement sheath, which provides mechanical support, ensures zonal isolation, and protects the casing from corrosive fluids. In high-temperature (HT) conditions, the cement must endure significant thermal and mechanical stresses, which can lead to plastic deformation, microcracking, and eventual failure, compromising well integrity.

Portland based cement (API Class G and H cement) are **conventionally** used for **cementing** geothermal wells (Guerrero, 1998). In recent decades, more advanced cements as Calcium Aluminate Cement (Vrålstad et al. 2021, Pytatian and Sugama. 2018) and ThermaLock were developed for high temperature geothermal applications. One of the main purposes of these cement solutions is to protect the casing strings and to ensure well integrity. To maintain its mechanical integrity under high temperature loading in geothermal wells, these cement solutions are designed to have sufficient strength. These cement solutions, with their designed strength and stiffness, significantly **restrain casing expansion** in radial and axial direction when heating up, resulting in **high thermal stresses in the casing**, see Figure 2. The high stresses in casing can lead to casing failure as seen in many high temperature wells in the past (Kruszewski and Wittig, 2018).

Foam cement solutions are instead a good solution for HT geothermal wells. Due to their remarkable advantages, namely low density, lower stiffness, high ductility, and compressibility, it provides a good solution to prevent losses when drilling and mitigate thermal stresses in the casing by increasing the flexibility in the well system (see Figure 1). Foam cement is a gas-liquid dispersion created when a gas, typically nitrogen, is stabilized as microscopic bubbles within a cement slurry (Harms and Febus, 1985). Nitrogen gas can be considered inert and does not react with or modify the cement-hydration product formation. Under special circumstances, compressed air can be used instead of nitrogen to create foamed cement (Crook, 2006). The small, fine foam bubbles are believed to promote stronger cement walls around the bubbles and to provide a set cement of increased integrity. The volumetric percentage of gas entrained in the foamed cement is referred to as the “foam quality” (e.g., 20% foam quality contains 20% entrained gas by volume, see Figure 2 for illustration of different foam qualities). Foam cement is a lower density cement system typically used in applications where the formation is unable to support the annular hydrostatic pressure of conventional cement slurries. In addition, their thermal conductivity is low, which helps reducing loss of energy when harvesting the reservoirs. F**oam cement** could be designed using **any type of cement base**, such as a Portland cement base or a calcium aluminate base, which makes it **versatile**. properties. By providing more accurate predictions of cement behaviour in extreme environments, this model supports the development of more resilient geothermal systems, enabling safer and more efficient energy extraction from super-hot geothermal reservoirs. In this work, the effects of mechanical properties of foam cements on well integrity are numerically studied. An advanced well-cement model is proposed and implemented in the stand-alone software CASINTEG (Hoang et al. 2021) for more reliable HT well design. The model integrates essential features, such as plasticity, pore pressure, and temperature-dependent properties, which are critical for understanding the interplay of mechanisms affecting cement integrity. A simplified Drucker-Prager-Cap model is adapted to simulate plasticity and potential compaction of the set cement under HPHT conditions.

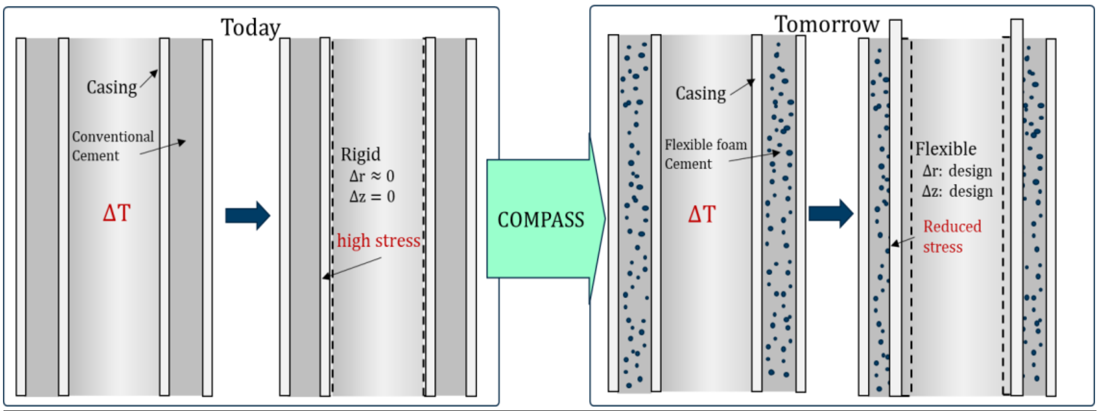

Figure 1: Illustration of thermal stress mitigation using foam cement.

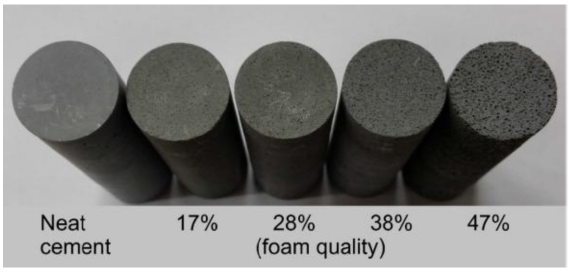

Figure 2: Illustration of neat cement samples (1 in. diameter) and foam cement (H type) with different foam quality (Haljasmaa et al. 2019).

Foam cement was originally developed and used for cementing O&G wells. Successful use of lightweight foamed cement in O&G applications was already documented in literature (Benge and Poole, 2005; Harlan et al., 2001; White et al., 2000; Kopp et al., 2000; Frisch et al., 1999; Benge et al., 1996; Harms and Febus, 1985). More recently, the use of foam cement in geothermal wells was also attempted, for example on Hawaiian geothermal well as reported by Bour and Richard (2020).

Reliable modelling of cement performance under HT conditions is essential for assessing well integrity and supporting safe well design. It is important to account for non-linear behaviours and key physical phenomena, such as transient heat transfer within the well and the temperature dependence of material

2. CONSTITUTIVE MODEL OF WELL CEMENT

After the cement slurry is pumped to fill the well annulus, the cement hydration process starts and there is a phase change from liquid to solid at percolation time t_p. The hydration process continues and is accompanied by a volumetric change (i.e. shrinkage or swelling). During the cement hydration, hydration heat is generated at a rate Q_h which varies with time. The hydration heat rate starts slowing down after its peak until the hydration reaction stabilizes at the so-called plateau time t_{pl}. Figure 3 illustrates the different phases of well cases.

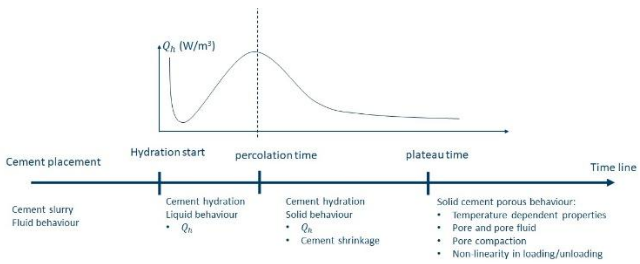

Figure 3. Illustration of time-dependent properties of cement.

In CASINTEG, set cement behaviour after hydration is modelled as solid material adopting a poro-plasticity behaviour. The strain tensor in cement can be decomposed as:

$$\boldsymbol{\varepsilon} = \boldsymbol{\varepsilon}_i + \boldsymbol{\varepsilon}_\tau + \boldsymbol{\varepsilon}_e + \boldsymbol{\varepsilon}_{hyd} + \boldsymbol{\varepsilon}_p \qquad (1)$$

where $\boldsymbol{\varepsilon}_\tau$, $\boldsymbol{\varepsilon}_e$, $\boldsymbol{\varepsilon}_p$ and $\boldsymbol{\varepsilon}_{hyd}$ are respectively the thermal, elastic, plastic and hydration strain tensors. While $\boldsymbol{\varepsilon}_i$ is the initial strain tensor which is the memory of cement state at the percolation time, deduced from the stress tensor in cement slurry at a given depth, z. The latter is written as:

$$\boldsymbol{\sigma} = -P\mathbf{I} = -\rho_s g z \mathbf{I} \qquad (2)$$

where ρ_s and g are respectively the density of slurry and specific gravity, while $\mathbf{I}$ is the second order unity tensor.

When setting, the stress tensor of solid cement can be decomposed as:

$$\boldsymbol{\sigma} = \mathbf{S} + \frac{1}{3} tr(\boldsymbol{\sigma})\mathbf{I} = \mathbf{S} + p\mathbf{I} \qquad (3)$$

where $\mathbf{S}$ is the deviatoric stress tensor, while p is the mean stress, responsible for cement compaction.

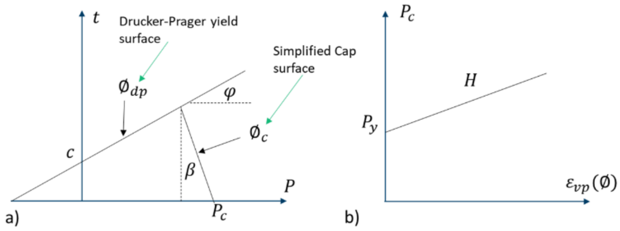

Figure 4. a) Drucker-Prager and simplified Cap yield surface and b) compaction yielding behaviour of set cement.

The plastic behaviour of cement is represented by the two-yield surface Drucker-Prager-Cap model as illustrated in 4 and written as follows:

$$\phi_{dp} = t + p\tan(\varphi) - c \qquad (4)$$

In these equations, t and p are respectively the Mises equivalent stress and the mean stress of the stress tensor, written as follows:

$$t = \sqrt{\frac{3}{2}\mathbf{S}:\mathbf{S}} \ and \ p = \frac{1}{3} tr(\boldsymbol{\sigma}) \qquad (5)$$

While φ and c are respectively the friction angle, and cohesion of the cement. Assuming perfect plasticity in shear (i.e., no hardening is caused by deviatoric stress), the cohesion value is a material parameter dependent only on the temperature. To model the compaction behaviour cement, a simplified cap yield surface was used and expressed as follows:

$$\phi_c = \tan(\beta)t - p - P_c \qquad (6)$$

where β is the cap angle and P_c the compaction pressure, defining the shape of the Cap yield surface. A linear hardening law is used to model the compaction behaviour of cement, as illustrated in **Error! Reference source not found.**b. The hardening law is the function relating the compaction yield stress, P_c, to volumetric inelastic strain ε_{vp} by:

$$P_c = P_y - H\varepsilon_{vp} \qquad (7)$$

in which P_y and H are respectively the initial yield stress and compaction hardening moduli.

The volumetric inelastic strain ε_{vp} is negative in compaction, and written as follows:

$$\varepsilon_{vp} = tr(\boldsymbol{\varepsilon}_\mathbf{p}) \qquad (8)$$

3. NUMERICAL MODEL OF WELL SEGMENT

To investigate the effect of the well cement model, FEA models of a 12m long well segment, consisting of casing, cement and formation multi-layers, were established in CASINTEG, see Figure 5a for illustration. The casing string is 12mm thick, while the cement sheath thickness is determined by the casing geometry and drill bit geometry. Three and five elements through thickness were used to model the casing and cement, as illustrated in Figure 5b. The rock radius is 10m, sufficiently large to model the far field condition. The established model geometry is summarized in Table 1.

Table 1: Model geometry.

Outer diameter (OD)	Casing OD (inch)	Drill bit OD (inch)	Rock OD (m)
Casing	9” 5/8	12” 1/4	10

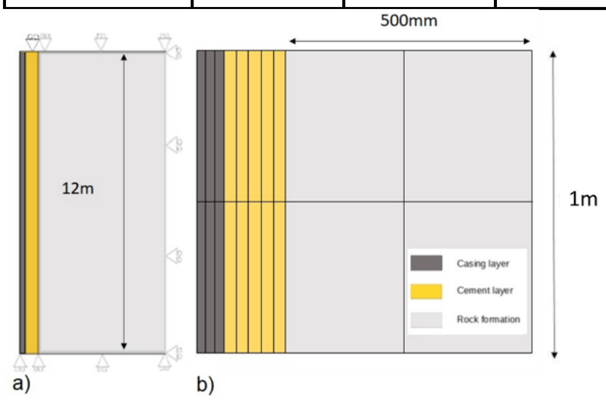

Figure 5. a) Casing segment models (12m long) and b) Illustration of meshed model

The cement is modelled by the constitutive equations described in Section 2. In the present work, the focus is on studying the effects of cement mechanical properties on the well behaviour under temperature loading. The effect of cement slurry and hydration is neglected. This means that $\boldsymbol{\varepsilon}_i$ and $\boldsymbol{\varepsilon}_{hyd}$ in Equations 1-2 are not considered in the present study. Typical thermo-mechanical properties of casing, cement, rock materials can be found in Table 2.

Table 2: Material parameters.

Materials	Casing steel	Cement	Rock
Young modulus (GPa)	210	10	50
Poisson's ratio	0.30	0.15	0.3
Thermal Expansion (10-6/K)	12	10	5.4
Density (kg/cm3)	7800	1900	2650
Specific heat (J/kg/K)	400	880	840
Thermal Conductivity (W/m/K)	50.4	0.81	2.0

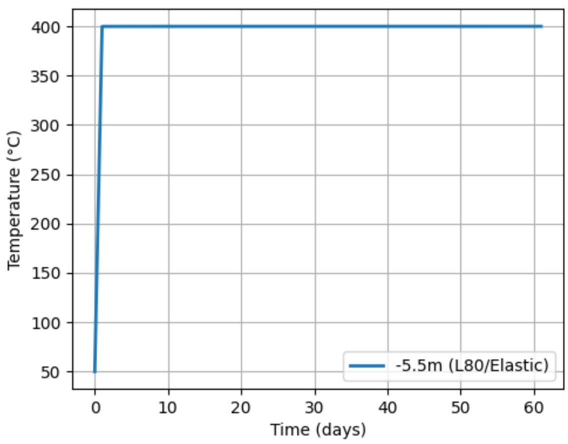

Figure 6. Temperature loading in the wellbore (on the casing inner surface)

The casing material is modelled using a thermo-elastic model. A typical API carbon steel is used for casing. The rock is also assumed to adopt a thermo-elastic behavior, and the radial displacement of the end rock was constrained, see Figure 5a for illustration. The bottom and top of the whole model were constrained in the axial displacement, except for the production casing string. The initial temperature in the whole model was set homogeneously at 50°C. A temperature load, ramping from 50°C to 400°C for one day, staying constant at 400°C for 60 days was applied to the inner surface of the casing, see Figure 6.

4. NUMERICAL RESULTS

4.1. Reference model

In this reference simulation, the material test data of API Porland G found in the work by Lima et al. (2022) are used to calibrate the yield parameters. Figure 7 shows the calibrated Drucker-Prager-simplified Cap yield surfaces, and the calibrated parameters are summarized in Table 3. Due to the lack of data about the hardening modulus, a small value $H = 1$ (GPa) in comparison to the Young's modulus is used in this present study.

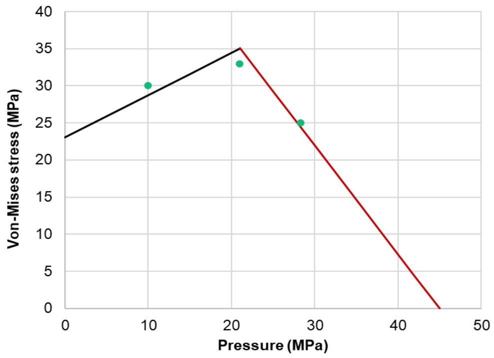

Figure 7. Illustration of calibrated Drucker-Prager-simplified Cap yield surfaces. The dotted points represent the test data from Lima et al. 2022.

Table 3: Yield function parameters for typical Porland G cement (Lima et al. 2022).

Yield function parameters	Value
Cohesion, C (MPa)	23
Friction angle, φ (rad)	0.52
Compaction yield pressure, P_y (MPa)	45
Cap angle, β (rad)	0.62
Compaction hardening modulus, H (GPa)	1

Figure 8 shows the simulated temperature evolution in the well segment at different simulation times. It can be seen that after 30 days the temperature in the model has almost reached the steady state.

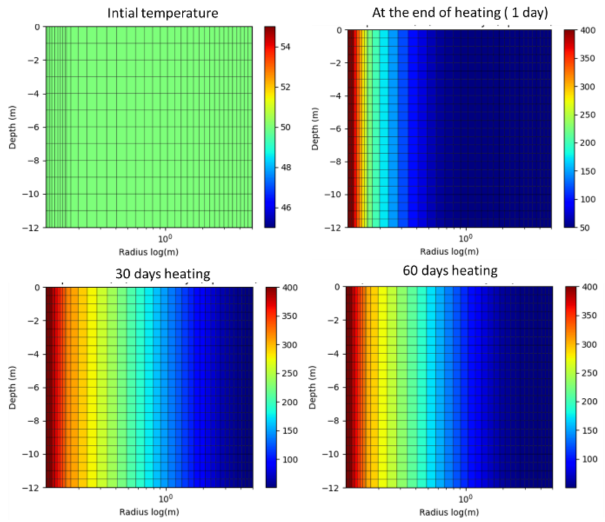

Figure 8. Evolution of temperature in the model as function of simulated time.

The stress path of the cement during heating is shown in Figure 9, alongside the initial yield surface. As the cement heats up, its stress condition reaches the compaction cap yield surface. The cement hardens under compaction, in accordance with the hardening modulus (H), leading to an expansion of the yield surface.

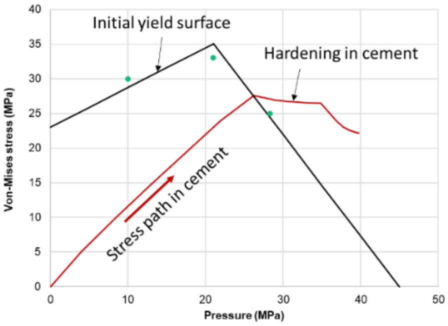

Figure 9. Stress path of cement (middle layer) during heating, plotted along with initial yield surface.

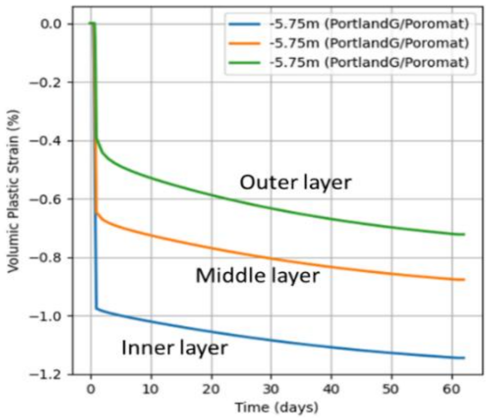

Figure 10. Volumetric plastic strain in cement (*Inner layer is in contact with casing, outer layer with rock*).

Figure 10 shows the evolution of volumetric plastic strain in the cement as a function of time. It is important to note that negative values represent volume compaction. The closer the cement is to the casing, the greater the plastic compaction experienced by the cement.

4.2. Influence of compaction yield pressure

In this section, the effects of the compaction yield pressure, P_y, are investigated. Simulations with P_y=15 MPa and 25 MPa are run, while keeping the other parameters consistent with the reference case. Figure 11 illustrates the effect of compaction yield pressure on cement stress and contact pressure at the casing/cement interface. In Subplot (a), the equivalent Von-Mises stress increases with pressure, indicating that higher P_y (45 MPa) leads to later plastic yielding in the cement. Conversely, lower P_y values (15 MPa and 25 MPa) result in earlier yielding during well heating, indicating more compaction. Subplot (b) shows that the contact pressure on the casing is lower for lower P_y, suggesting a reduced risk of casing collapse during well heating.

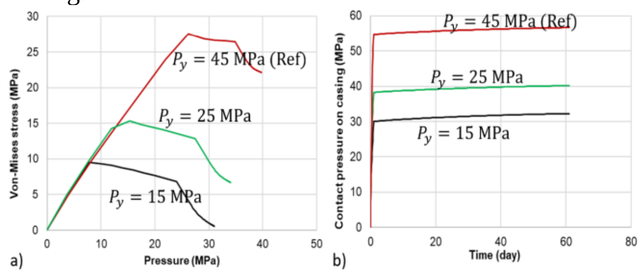

Figure 11. Effect of yield pressure P_y on a) Stress evolution in cement (mid-layer) and b) Contact pressure on the casing at the casing/cement interface

Figure 10 shows the influence of P_y on cement compaction in the cement layers. The results indicate that a lower compaction pressure not only increases the plastic volumetric strain but also makes the compaction more homogeneous throughout the cement thickness. These results highlight that cement with lower yield pressures promotes gradual, homogeneous compaction, which enhances the well's flexibility and reduces the risk of casing collapse.

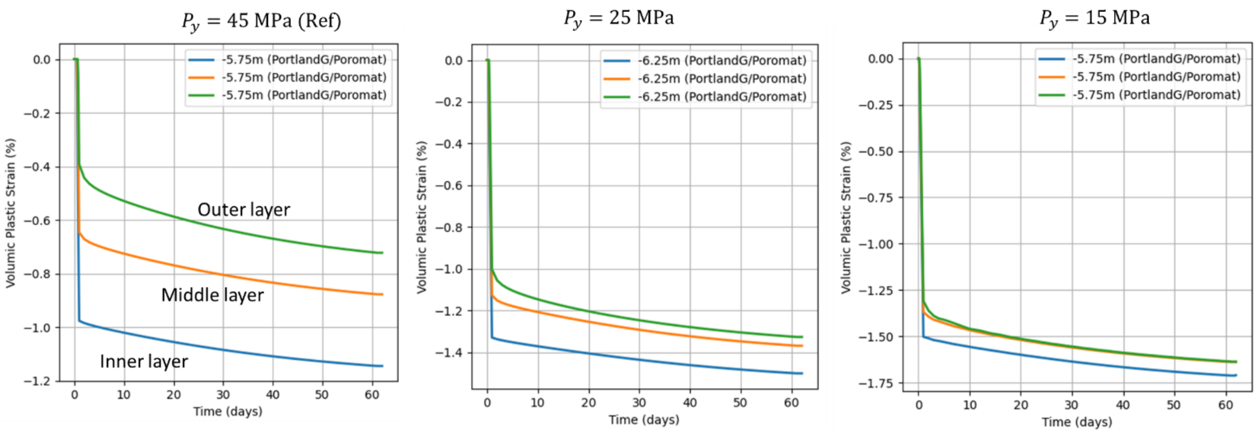

Figure 12: Effect of compaction yield pressure P_y on volumetric plastic strain in cement (*Inner layer is in contact with casing, outer layer with rock*).

4.3. Influence of Hardening Modulus

In this Section, the effects of cement hardening modulus, H, are investigated. Simulations with H=0.1GPa and 0.5GPa are runs, while keeping the other parameters as in the reference case. Figure 13 shows the influence of H on cement stress and contact pressure at the casing/cement interface.

As shown in Figure 13a, when heating, the stress in cement evolves and reaches the same yielding point for the investigated cases. However, as the hardening modulus decreases, the cement becomes softer under higher compaction pressure. Figure 13b shows that lower H values also result in lower and slower increases in contact pressure, implying a reduced risk of casing collapse during well heating due to less rapid compaction.

Figure 14 shows the influence of H on cement compaction in the cement layers. The results indicate that a lower hardening modulus leads to higher volumetric plastic strain in the cement layers close to the casing surface, while it decreases as we move outward toward the rock surface. This depicts that the radial expansion of the casing during heating is primarily accommodated by the compaction of the cement layers near the casing surface, when the hardening modulus is reduced.

These results suggest that using cement with a lower hardening modulus can enhance the flexibility of the cement layer, helping to mitigate the risk of casing damage during thermal cycling, similar to the effects observed with lower yield pressures in the previous section.

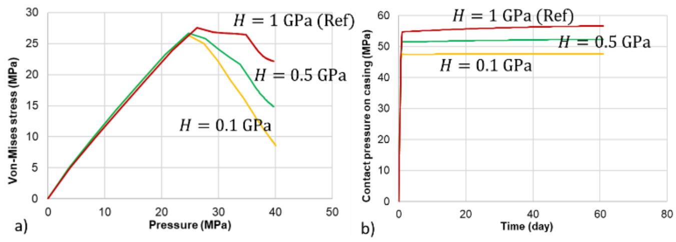

Figure 13. Effect of hardening modulus H on a) Stress evolution in cement (mid-layer) and b) Contact pressure at the casing/cement interface.

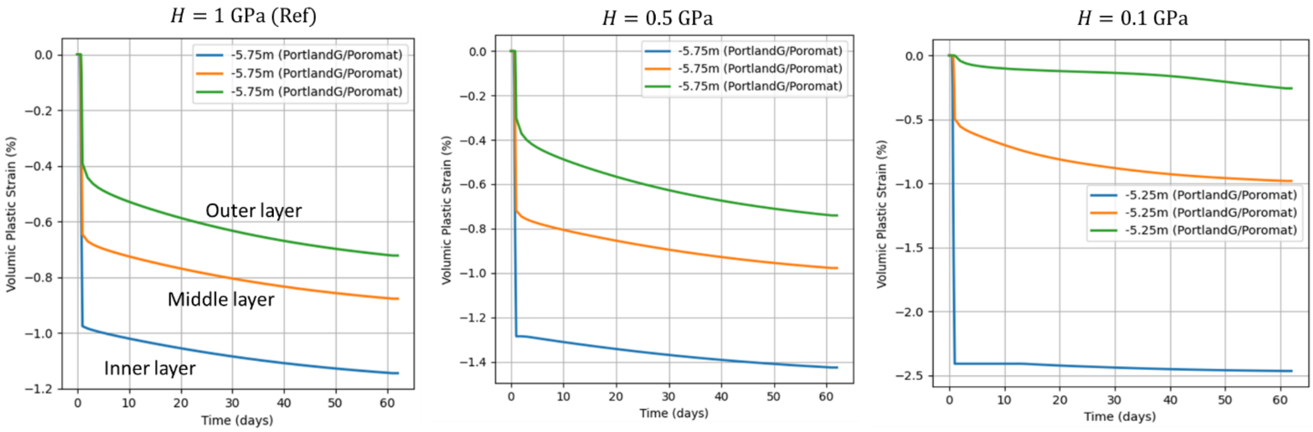

Figure 14: Effect of hardening modulus H on volumetric plastic strain in cement. (*Inner layer is in contact with casing, outer layer with rock).*

4.4. Effects of the foam cement properties

The foam cement exhibits lower Young's modulus, lower compaction yield pressure, and lower hardening modulus compared to conventional cement. To simulate the effects of foam cement, simulations are conducted with lower values for these parameters: Young's modulus $E = 2.5$ GPa, hardening modulus $H = 0.5$ GPa with $P_y = 15$ MPa and $P_y = 10$ MPa. The simulation results, in terms of contact pressure at the casing/cement interface, are shown in Figure 15, alongside the reference case using conventional Portland cement. It can be seen that foam cement significantly reduces the pressure on the casing, thereby mitigating the risk of casing collapse during thermal cycling. This effect is attributed to the foam cement's softer, more flexible characteristics, which allow it to better accommodate radial expansion during heating.

The higher volumetric plastic strain, as shown in Figure 16, further confirms that foam cement undergoes greater deformation under compaction compared to conventional cement. This increased strain is consistent with the lower hardening modulus and yield pressure of foam cement, which allows for more plastic deformation. The results highlight that foam cement not only reduces the contact pressure on the casing but also accommodates higher strain, contributing to better flexibility and reduced risk of casing damage during thermal cycling.

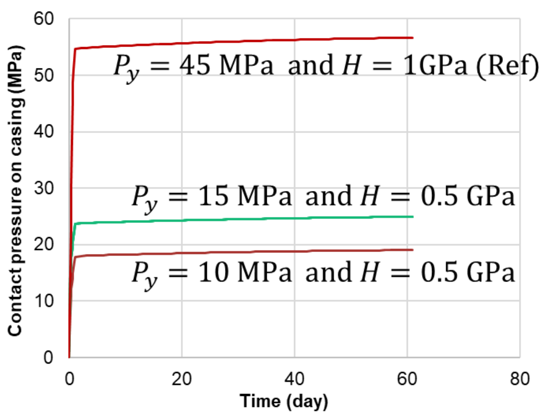

Figure 15. Effect of foam cement properties on contact pressure at the casing/cement interface.

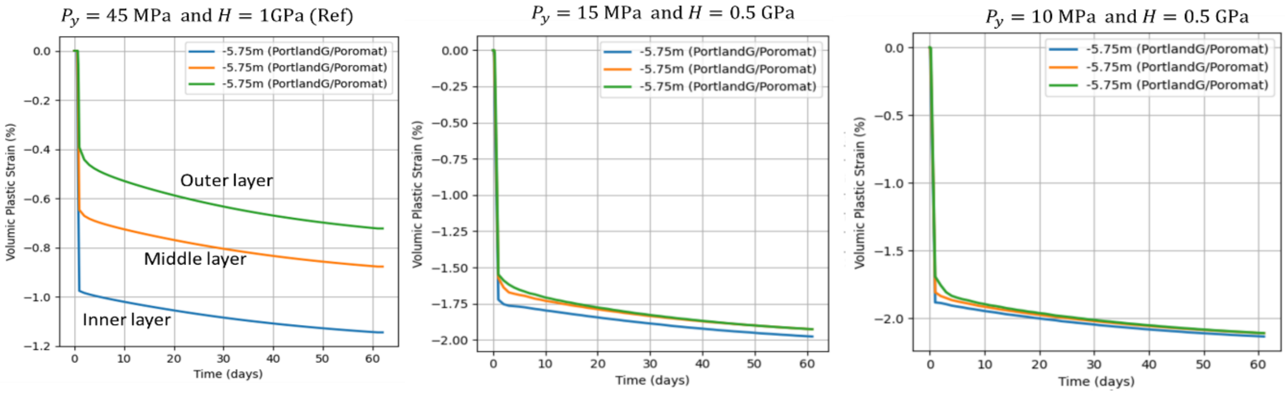

Figure 16: Effect of foam cement properties on volumetric plastic strain in cement (*Inner layer is in contact with casing, outer layer with rock).*

5. CONCLUDING REMARKS

The construction of robust geothermal wells, particularly those tapping into superhot geothermal reservoirs, is essential for the sustainable production of energy. Cement, acting as the main barrier for casing integrity, is a critical component for ensuring well stability. Maintaining well integrity under high-temperature conditions still remains a challenge. Foam cement, with its lower stiffness, enhanced ductility, and reduced yield pressure, provides a viable solution for ensuring well integrity by reducing thermal stresses and accommodating casing expansion.

The results presented here demonstrate that foam cement reduces contact pressure at the casing/cement interface, thereby potentially lowering the risk of casing collapse during thermal cycling. The ability of foam cement to undergo more homogeneous compaction, particularly under high compaction pressures, enhances the well's flexibility and overall performance.

However, for further optimization and validation of these results, additional data and advanced models are required. For accurate structural analysis of geothermal wells, obtaining realistic stress states in the cement after hydration is crucial as an initial condition prior to the warm-up phase. Although the chemical hydration process is not explicitly modelled, its effects on the initial stress in the set cement are captured by accounting for changes in mechanical properties throughout the curing process. Future work should focus on incorporating the hydration effects on cement behavior, which significantly impact the long-term performance of the material in high-temperature environments. The inclusion of realistic field conditions is necessary to improve the accuracy of predictive models. Ultimately, reliable data and robust models will be essential to advancing the design and integrity assessment of geothermal wells, ensuring safer and more efficient energy extraction from superhot geothermal reservoirs.

ACKNOWLEDGEMENTS

This work was supported by the Horizon Europe research and innovation programs under grant agreement No. 101084623 (COMPASS). The authors thank all project partners and contributors.

REFERENCES

Guerrero. "Cementing Of Geothermal Wells." The United Nations Uni, Geothermal Training Programme, Reykjavik, Iceland (1998).

Vrålstad, Torbjørn, et al. International Conference OMAE. Vol. 85208. ASME, 2021

Pytatian and Sugama 2018: Cements for high-temperature geothermal wells.

Harms, W. M.; Febus, J. S. Cementing of fragile-formation wells with foamed cement slurries. Journal of Petroleum Technology 1985, 37, 1049–1057.

Crook, R., 2006: Cementing. Chapter 9 in: Lake, L.W., and Mitchell, R.F. (eds.), Petroleum engineering handbook, vol. II: Drilling engineering. Society of Petroleum Engineers, Richardson, Texas, 369-431.

Benge, O. G.; McDermott, J. R.; Langlinais, J. C.; Griffith, J. E. Foamed cement job successful in deep HTHP offshore well. Oil and Gas Journal 1996, 94, 58–63.

Benge, G.; Poole, D. Use of foamed cement in deep water Angola; SPE/IADC Drilling Conference in Amsterdam, The Netherlands, Feb 23–25, 2005; SPE/IADC 91662.

White, J.; Moore, S.; Miller, M.; Faul, R. Foaming cement as a deterrent to compaction damage in deepwater production. IADC/SPE Drilling Conference, New Orleans, LA, Feb 23–25, 2000; IADC/SPE 59136.

Kopp, K.; Reed, S.; Foreman, J.; Carty, B.; Griffith, J. Foamed cement vs. conventional cement for zonal isolation – case histories. SPE Annual Technical Conference and Exhibition, Dallas, TX, Oct 1–4, 2000; SPE 62895.

Frisch, G. J.; Graham, W. L.; Griffith, J. Assessment of foamed-cement slurries using conventional cement evaluation logs and improved interpretation methods. Presented at the 1999 SPE Rocky Mountain Regional Meeting, Gillette, WY, May 15–18, 1999; SPE 55649.

Haljasmaa, I., Kutchko, B., Spaulding, R., Crandall, D., Moore, J., Gill, M., Benge, G., Hawthorne, S.B., Dockter, B.A., Beddoe, C. and Sorensen, J., 2019. *Foamed Cement: Correlation of Foam Quality with Mechanical and Physical Properties* (No. e7885994-277c-45e3-944a-8ebb23b9ed8d). National Energy Technology Laboratory (NETL)

Bour, D. and Rickard, B., 2000. Application of foamed cement on Hawaiian geothermal well. TRANSACTIONS-GEOTHERMAL RESOURCES COUNCIL, pp.55-60. Pittsburgh, PA, Morgantown, WV (United States).

Hoang, N.H., Mainçon, P., Philippe, D., Coudert, T., Bjørset, A. and Sæther, S., 2021. Novel computational tool for efficient structural analyses of geothermal wells. Geothermics, 92, p.102058.

Lima, V. N., Skadsem, H. J., Beltrán-Jiménez, K., Zhemchuzhnikov, A., Velloso, R. Q., & de Andrade Silva, F. (2022). Triaxial behavior of a stabilized and a highly porous oil well cement paste at different saturation and drainage conditions. *Journal of Petroleum Science and Engineering*, *219*, 111055.